

Carbonate Coprecipitation for Cd and Zn Treatment and Evaluation of Heavy Metal Stability Under Acidic Conditions

Julie J. Kim, Sang Soo Lee, Paul Fenter, Satish C. B. Myneni, Viktor Nikitin, and Catherine A. Peters*

Cite This: *Environ. Sci. Technol.* 2023, 57, 3104–3113

Read Online

ACCESS |

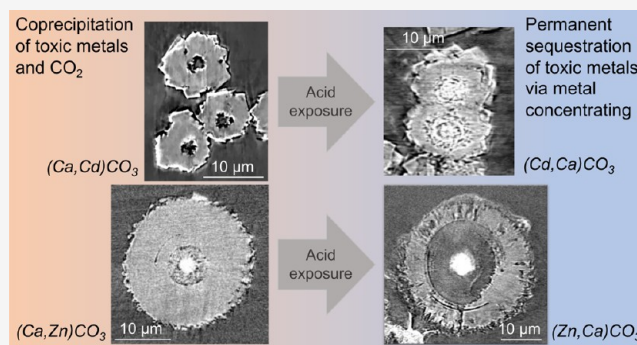
Metrics & More

Article Recommendations

Supporting Information

ABSTRACT: Mining wastes or combustion ash are materials of high carbon sequestration potential but are also known for their toxicity in terms of heavy metal content. To utilize such waste materials for engineered carbon mineralization purposes, there is a need to investigate the fate and mobility of toxic metals. This is a study of the coprecipitation of metals with calcium carbonate for environmental heavy metal mitigation. The study also examines the stability of precipitated phases under environmentally relevant acid conditions. For a wide range of cadmium (Cd) and zinc (Zn) concentrations (10 to 5000 mg/L), induced coprecipitation led to greater than 99% uptake from water. The calcium carbonate phases were found to contain amounts as high as 9.9 wt % (Cd) and 17 wt % (Zn), as determined by novel synchrotron techniques, including X-ray fluorescence element mapping and three-dimensional (3D) nanotransmission X-ray microscopy (TXM). TXM imaging revealed first-of-a-kind observations of chemical gradients and internal nanoporosity within particles. These observations provided new insights into the mechanisms leading to the retention of coprecipitated heavy metals during the dissolution of calcite in acidic (pH 4) solutions. These observations highlight the feasibility of utilizing carbonate coprecipitation as an engineered approach to the durable sequestration of toxic metals.

KEYWORDS: carbon mineralization, water treatment, calcium carbonate, cadmium, zinc, CO₂ sequestration, X-ray computed tomography, acid leaching



1. INTRODUCTION

Release of hazardous runoff such as mine drainage or combustion ash leachate poses environmental threats to water resources as they contain high levels of toxic elements such as cadmium (Cd), zinc (Zn), and other contaminants (i.e., arsenic, chromium, selenium, etc.).^{1,2} Cadmium is a known carcinogen and can negatively impact neurological, reproductive, and respiratory systems. While Zn is an essential nutrient for humans at appropriate levels, excess exposure can cause health problems and is especially hazardous to children. Zinc also commonly co-occurs with Cd, increasing the likelihood of finding excess Zn concentrations in hazardous waste streams.^{3–5} Environmentally observed concentrations of Cd and Zn range from a few ppm to millions of ppm, and these are levels that far exceed national primary and secondary drinking water standards (Maximum Contaminant Levels, MCL) set by the U.S. EPA (Figure 1). The pH conditions of these solutions cover acidic to alkaline regimes, causing additional environmental concerns. While there are extensive in-situ and passive treatment efforts to minimize toxic metal concentrations and ameliorate extreme pH conditions including limestone drains, permeable reactive barriers, and constructed wetlands,^{6–8} these technologies alone are not

enough to achieve complete mitigation of contaminants or pH recovery.

Despite these environmental concerns, some combustion, mining, and other alkaline industrial wastes can provide environmental benefits because of their cation content,^{9–11} mainly in the form of Ca²⁺, Mg²⁺, and Fe²⁺, which can precipitate as carbonate minerals, thereby acting as a sink for CO₂ gas in the Earth's atmosphere. For example, the global annual potentials for CO₂ capture were found to be 4.5 Gt for ultramafic mine tailings¹² and 0.2 Gt for coal ash,¹³ suggesting that alkaline wastes may contribute significantly to achieving net negative emissions.¹³ A wealth of literature has quantified the kinetics of carbonation reactions, availability of waste materials, economic feasibility, and heat potentials^{12–18} in the context of CO₂ sequestration efforts. It remains to be seen whether engineered carbon mineralization processes can offer

Received: October 18, 2022

Revised: January 4, 2023

Accepted: January 5, 2023

Published: February 13, 2023



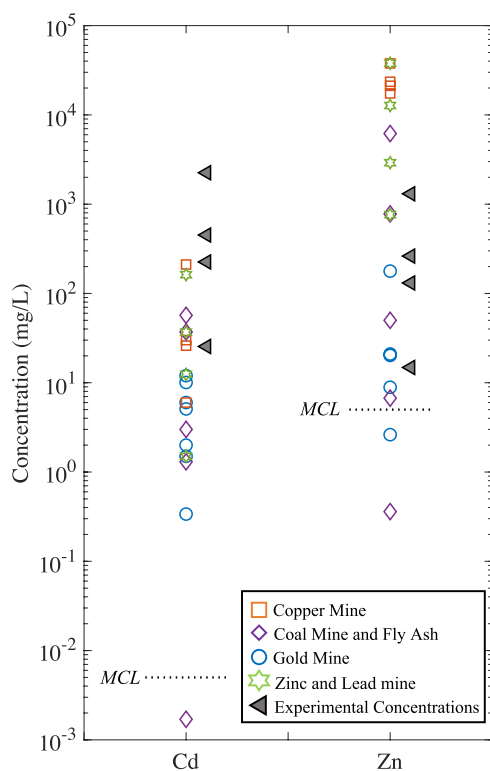


Figure 1. Cadmium and Zn concentrations in various mining waste and combustion ash runoff waters and leachates. Triangle markers (black) indicate the concentrations explored in this study. The horizontal dotted lines indicate the National Primary or Secondary Drinking Water standards (MCL) set by the U.S. EPA. Data were compiled from various sources.^{3–5,11,43–48}

permanent and simultaneous sequestration of both CO₂ and heavy metals.

In this work, we addressed the following research questions: to what extent can carbonation reactions sequester heavy metals through coprecipitation in highly contaminated solutions and what is the fate of the heavy metals if the carbonate solids were to start dissolving? These are topics starting to get attention in the context of calcium carbonate coprecipitation as a possible heavy metal sequestration approach in various environmental remediation scenarios including mine wastes, nuclear waste repositories, or contaminated aquifers.^{19–24} Precipitation of calcite and incorporation of Cd or Zn in well-controlled settings has been well studied.^{25–30} In cationic coprecipitation, heavy metals that exist as dissolved divalent cations can substitute for the major cations in a host carbonate phase.^{20,26–33} This phenomenon is explained by the solid solution–aqueous solution (SS–AS) theory,²⁵ and the tendency of coprecipitation is controlled by a number of factors. In the systems of

Ca–Cd or Ca–Zn pairs, calcite (the most stable polymorph of calcium carbonate) is more soluble than both Cd- and Zn-carbonate endmembers, otavite (CdCO₃) and smithsonite (ZnCO₃), respectively (Table 1). Because these solid phases belong to the same crystal group of rhombohedral carbonates, the degree of interstitial mixing is controlled by the relative size of the cations. Cadmium ions have a similar ionic radius to Ca ions (94 vs 100 pm, respectively), whereas Zn ions are significantly smaller (74 pm), making these elements compatible with calcite. As a result, otavite can form a continuous solid solution with calcite for all possible mole fractions,³⁴ whereas smithsonite forms a solid solution with calcite with immiscibility above 0.2 mole fraction.³⁵ Factors such as the ratio of the solubility products, the distribution coefficient,^{27,29} the degree of supersaturation, temperature, nucleation rates, charge similarity, and metal complexes³⁰ influence the extent of metal incorporation. Building on this foundational knowledge, this work attempts to better understand the coprecipitation process in an environmental remediation sense, focusing on the potential for heavy metal uptake from the aqueous phase and the fate of heavy metals in calcite.

Unique to this investigation is the use of synchrotron-based absorption contrast transmission X-ray microscopy (TXM), which is a form of X-ray computed tomography (XCT) for three-dimensional (3D) imaging. The use of TXM imaging in this study enabled first-of-a-kind observations of internal structures and compositions of coprecipitates at nanometer resolution. These methods are analogous to those that have revealed compositionally heterogeneous solids in natural and engineered systems^{36–39} and the spatial distribution of foreign ions within particles, the particle substructure, and its impact on the morphology of precipitates.^{33,40–42} Here, we used these methods to elucidate mechanisms of calcite coprecipitation, such as the order of precipitation, and physical internal structure evolution. The aim was to use these novel observations to ultimately advance utilization of carbonate coprecipitation as a technology for simultaneous heavy metal and CO₂ sequestration.

This study investigated coprecipitation of Cd and Zn in calcium carbonate for a wide but relevant range of concentrations consistent with observed concentrations in mining and coal combustion waste runoff and leachates (Figure 1). The efficiency of coprecipitation reactions for removing toxic metals from the water was evaluated for solutions that were supersaturated with respect to calcium carbonate. Inferences about trace element incorporation in the coprecipitated carbonate phases and effects on morphology, crystal structure, and chemical composition were obtained using TXM and XRF imaging as well as standard methods for mineral characterization.

Table 1. Summary of Theoretical Metal Solubilities in Water and in Acidic Solution at pH 4 for Different Endmember Carbonates

mineral	K_{sp} ^a	aqueous solubility of the metal (mol/L) in pure water ^b	aqueous solubility of the metal (mol/L) in a fixed pH 4 solution
CaCO ₃ (calcite)	10 ^{-8.48}	1.2 × 10 ⁻⁴ (12 mg/L)	1.4 × 10 ⁰ (140,000 mg/L)
ZnCO ₃ (smithsonite)	10 ⁻¹⁰	6.1 × 10 ⁻⁵ (7.6 mg/L)	6.0 × 10 ⁻¹ (75,240 mg/L)
CdCO ₃ (otavite)	10 ^{-12.10}	5.6 × 10 ⁻⁶ (0.9 mg/L)	6.3 × 10 ⁻² (10,862 mg/L)

^aSolubility product constants (K_{sp}) at 25 °C were taken from the WATEQ. 4F Database⁴⁹ and references therein. ^bAqueous solubilities were obtained from PHREEQC simulations. Calculations were done for a closed system.

This study also investigated the stability of the heavy metals in the coprecipitated carbonate phases. Carbonate minerals are relatively stable at neutral and alkaline pH but are thermodynamically unstable and readily dissolve in acidic conditions, as shown in Table 1. This was the motivation to study the extent to which heavy metals will be durably sequestered under conditions that would lead to dissolution of the host carbonate phase (e.g., will they be released into solution or remain incorporated in the solid?). Mildly acidic conditions (pH 4 to 6) are prevalent in various settings, such as natural bodies of water and rainwater, and thus, testing the coprecipitated carbonates under these conditions is important for environmental and engineered systems. While dissolution of calcite is widely studied and well understood, the effect of heavy metal presence and distribution on the dissolution processes remain to be better characterized.

2. MATERIALS AND METHODS

In this work, binary combinations of Ca with Cd and Ca with Zn were studied. Initial solutions were prepared by mixing stock solutions formulated with deionized water (refer to the Supporting Information for more details about the chemical composition, source, and purity of salts). For Cd, aqueous concentrations from 0.0002 mol/L (25 mg/L) to 0.02 mol/L (2250 mg/L) were studied, and for Zn, concentrations from 0.0002 mol/L (15 mg/L) to 0.02 mol/L (1300 mg/L) were studied (Figure 1). A single initial Ca concentration of 0.2 M was used for all experiments, and the molar ratio of Ca and carbonate was 1:1. This Ca concentration was chosen based on observed concentrations in waste leachates ranging from 200 to 15,000 mg/L.^{2,5} The initial pH was 11 by amendment with sodium hydroxide solution, which was adjusted because higher pH promotes calcite precipitation. An experiment without Cd or Zn was also conducted as the calcium carbonate control.

The resulting solution was supersaturated with respect to calcite (refer to the Supporting Information for additional details) and precipitates nucleated immediately after mixing, and the solids and solutions were equilibrated for 7 days. For comparison with measured solid composition values, PHREEQC simulations were done to predict the incorporation of Cd and Zn into the solid phase. The “solid solutions” function was used, which uses the SS–AS model and assumes ideality with respect to solid phase activity coefficients.

For the acid dissolution experiments, precipitated solids were mixed with 0.1 M hydrochloric acid (HCl) solution (pH of 4 +/−0.05) for 3 days. These experiments had a solid-to-solution ratio of 0.8 mg/mL, which was determined via preliminary experiments to ensure partial dissolution of the solids and so that the structure and chemical composition of the remaining solids could be analyzed.

In all batch experiments, reaction vessels were placed on a shaker table for 2–3 h and then set for quiescent equilibration. After the reaction, samples of the solution were drawn, filtered (0.7 μm pore, glass fiber filter), and acidified with 2% nitric acid. Aqueous samples were analyzed using inductively coupled plasma mass spectroscopy (ICP-MS) using a Thermo Neptune multicollector with detection limits in the ng/L range. Replicate experiments were conducted for all experiments, and average concentrations were reported. All precipitates collected were washed three times with deionized water and ethanol. To visualize morphology, solid precipitates were examined using scanning electron microscopy (SEM) (Phenom, Thermo Fisher Scientific).

To examine the internal structure, texture, and chemical gradients, individual particles were scanned in 3D using the TXM beamline of sector 32-ID-C at the Advanced Photon Source (APS).^{50,51} Precipitates were imaged at 8 keV energy to maximize contrast between Ca and Cd. Additional scans at 10 keV (slightly above the Zn X-ray absorption edge) were performed to maximize the contrast between Ca and Zn. Scan rates were between 0.5 and 1 s per angle, covering approximately 175°. Data were reconstructed using Tomopy,⁵² which has now been replaced with Tomocopy,⁵³ and visualized using ImageJ. The voxel resolution of the resulting 3D tomographic images was 56 nm. Phase segmentation was done using Dragonfly.

Select samples were analyzed for mineral composition using high-resolution powder X-ray diffraction (XRD) at APS beamline 11-BM. Each scan was taken in a 2θ range between 0.5 and 50° ($\lambda = 0.4582 \text{ \AA}$), with a step size of 0.001° and a time step of 0.1 s/step.

Solid precipitates were examined using micro X-ray fluorescence (μ XRF) at APS GSECARS beamline 13-ID-E to detect, map, and quantify trace element incorporation in the particles. Loose precipitates were mounted on a polyimide slide using epoxy and polished in-house to reveal a combination of cross-sections and intact particles. Areal scans of variable sizes containing multiple particles were taken at an incident energy of 18 keV, with a spatial resolution of 2 μm and a dwell time of 20 ms. Element maps were generated using Larch.⁵⁴ Quantitative analyses were done using the NIST NRLXRF tool, as shown previously,^{38,39} and assuming the host mineral phase forms a solid solution with calcite. Reported weight fractions are average values from nine different particles.

3. RESULTS AND DISCUSSION

3.1. Uptake of Heavy Metals from Solution. A primary indicator of the effectiveness of coprecipitation is the residual heavy metal concentrations in the aqueous phase after inducing carbonate precipitation. The measured aqueous Cd and Zn concentrations are reported in Figure 2. For all four experiments in the Zn series, residual concentrations were near to or below the MCL (5 mg/L), with at least a 99.5% decrease after precipitation. While the Cd concentrations after precipitation were still mostly above the MCL (5 μg/L), concentrations were reduced by at least 99.7%, and this demonstrates coprecipitation in carbonate as a highly efficient process for removal of toxic metals from solution.

The amount of Ca in solution determines the amount of precipitate, which ultimately affects the heavy metal uptake from solution. To examine this, we used the PHREEQC SS–AS model to simulate uptake for different amounts of Ca in solution (Figure S1). In the Cd-cases, at a Ca concentration of 0.8 g/L (which is also the concentration used here), approximately 2 g/L of coprecipitated solids is formed and >95% uptake of Cd is estimated. In the Zn-cases, at the same concentration of Ca, 85% uptake is estimated. There is a steep decrease in the heavy metal uptake for Ca concentrations below 0.8 mg/L. This means that for any system, there exists a minimum Ca concentration to achieve the desired final residual concentration and engineering this process will require careful attention to the initial cation content of the waste materials.

To maximize uptake, it is also important to control the Ca to carbonate ratio as this ratio controls the polymorphism of

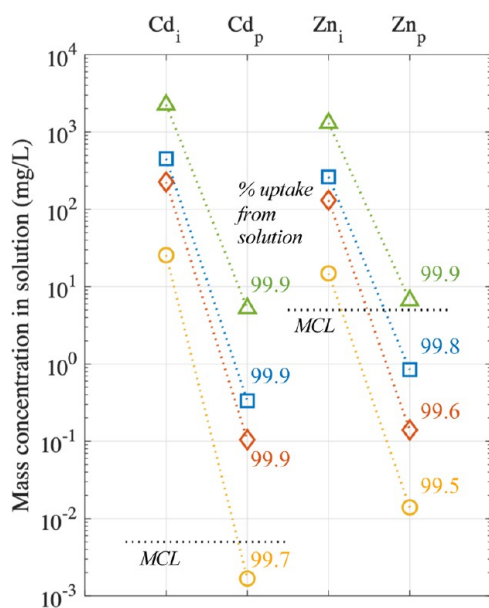


Figure 2. Aqueous heavy metal concentrations in the initial solution (with subscript i) and precipitating solution (with subscript p). Dotted horizontal lines are the national primary or secondary drinking water standards.

calcium carbonates, as well as the nucleation and growth rates, which in turn control the degree of coprecipitation.^{20,55} A cation–anion ratio of ~ 1 has been found to promote precipitation of the most stable calcium carbonate phase, calcite, and lead to the highest precipitation rates.⁵⁵ Control of such conditions may be significant to maximizing the uptake of heavy metals.

3.2. Solid Phase Analyses and Spatial Distributions of Heavy Metals in Calcite. Analyses of the solid-phase composition using XRD (Figure S3) showed that all precipitates formed in the presence of Cd and Zn exhibited only calcite peaks with no evidence of other carbonate phases such as otavite or smithsonite. This suggests precipitation of Cd-bearing calcite or Zn-bearing calcite of variable degrees of incorporation. Analysis of the peaks showed a systematic change in the lattice spacing, which supports the conclusion that heavy metals have become incorporated within the calcite crystal rather than adsorbed on the surface or forming its own end-member carbonate phase. We also observed a noticeable peak broadening with increasing Cd or Zn concentrations (Figure S4), which indicates the presence of microstrain, chemical variation, and changing crystallite size within the precipitated calcites.

SEM images were used to examine precipitate size and morphology. Calcite is known for its characteristic rhombohedral shape, and this was observed of the control (Figure S5) and of the low Cd and Zn cases (Figure 3). For higher Cd and Zn concentrations, the morphology was significantly altered, and the particles were aggregated. For higher Cd concentrations, the sizes of particles were smaller, with a majority of the precipitates measuring less than $10\ \mu\text{m}$. This may be due to an interplay of ion adsorption, a thin passivating layer of a Cd-rich phase or roughening of surfaces, all of which are factors that inhibit particle growth.^{56–58} In the Zn precipitates, the crystal morphology became more platy, especially at the highest concentrations, and this may be due to the adsorption of ions on growth sites, which can limit the rate of crystal

growth and alternatively promote topology and subsequent morphological changes in calcite precipitates.³⁰ Unlike the Cd cases, the particle sizes were significantly larger with higher Zn concentrations (some nearly $50\ \mu\text{m}$ in size), and in the highest concentration case, the calcite particles were nearly spherical with rough surface features, exhibiting morphology similar to that expected for vaterite precipitates. Nevertheless, the XRD results demonstrated that this remained calcite, suggesting that the large spherical grains are secondary assemblies of primary calcite particles. A minor Zn-carbonate hydroxide phase, hydrozincite ($\text{Zn}_5(\text{OH})_6(\text{CO}_3)_2$, $\log K_{\text{sp}} = -14.9$),⁵⁹ was observed as bright, nonspherical particles (Figure 3). This suggests that hydrozincite can serve as an additional carbonate sink for Zn, which is consistent with previous observations of hydrozincite formation in Zn-enriched environments.^{60,61}

Quantification of heavy metals in precipitates using averaged μXRF data compiled from multiple single particles yielded averages of 0.3 wt % (mole fraction 0.002) of Cd and 1.4 wt % (mole fraction 0.02) of Zn in the lowest concentrations and 9.9 wt % (mole fraction 0.09) of Cd and 17 wt % (mole fraction 0.28) of Zn in the highest concentrations, exceeding the limit of solubility of Zn in calcite. It was predicted that Cd uptake in calcite would be greater than Zn uptake simply based on the relative solubilities, yet the opposite was observed. This suggests that utilizing the solubilities of endmembers to predict the relative degree of uptake remains limited. PHREEQC SS–AS predictions were also compared to experimental observations (Figure S2), and for the observed aqueous concentrations, it was found that there are discrepancies between the measured and predicted Cd or Zn mole fractions in the solid, and these discrepancies are slightly more significant for Cd experiments than for Zn. These discrepancies may derive from the assumptions of the SS–AS model, making it potentially limited in capturing the actual growth kinetics for solid solutions especially in cases of precipitation from solutions that are highly supersaturated.²⁰ Furthermore, this model assumes precipitation of a single phase, which means some undetectable phases (i.e., those below the detection limit of XRD) may serve as sinks for the heavy metals, which are unaccountable in the SS–AS predictions, and precipitation of homogeneous solid solutions, whereas our observations, below, will show significant compositional and morphological variations in and within the precipitated solids.

Additional analyses will focus on the experiments with the highest Cd and Zn concentrations. Multiple particles were examined by generating μXRF element maps, which show elemental distributions and relative abundances using a red–green color scale, and further incorporate the information in depth as synchrotron X-rays can penetrate the sample. For the Cd case, the particles exhibited the presence of Cd homogeneously distributed within the particles (Figure 4a), and for Zn–calcite particles, a Zn-rich outer layer was sometimes observed (Figure 4e), along with a Zn-rich core (Figure 4f). Complementary TXM images revealed important, new features of the interiors of individual particles. Slices through the particles are shown in Figure 4, and animations of the particles in 3D are available as supplementary materials (Movies S1–S8 and Figures S12 and S13). In these images, brighter grayscale intensities indicate higher concentrations of the heavy metals. The low-concentration cases (Figure S6) were very similar to the calcite control, indicating either homogeneous distribution of trace elements or incorporation of the trace elements under detectable amounts. For Cd at the

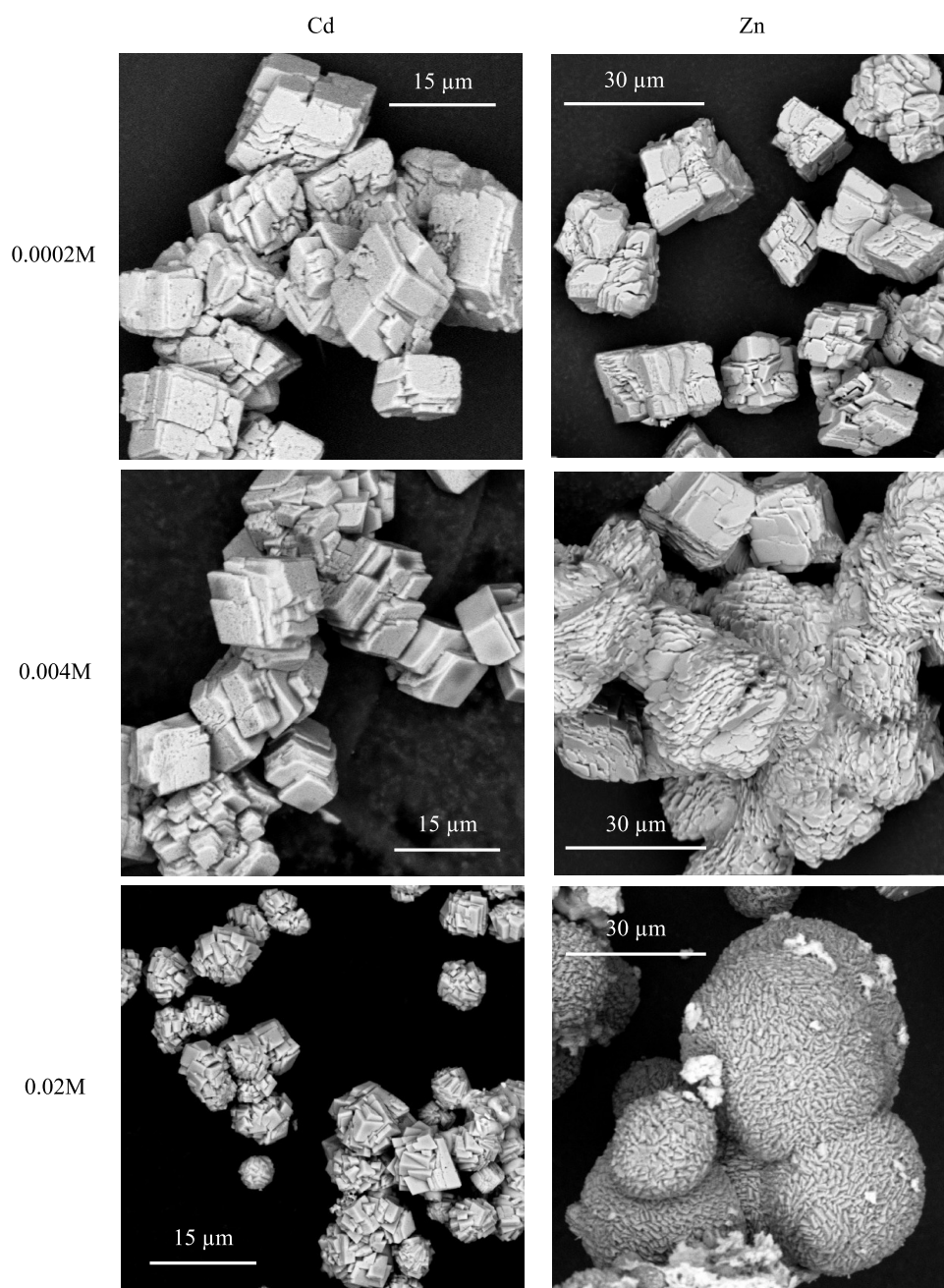


Figure 3. SEM images of calcium carbonate precipitates show changes in size and morphology for different initial Cd and Zn concentrations (0.0002–0.02 M). Calcite precipitates from the 0.002 M case are not shown.

highest concentration, a hollow center is clearly visualized (Figure 4c), which may be explained by early precipitation and subsequent dissolution of metastable amorphous calcium carbonate or the creation of CO₂ bubbles serving as a scaffold for crystal growth.^{62,63} A high-density Cd-rich outermost layer at the external solid–air interface was also observed (Figures 4c and S7a), but it is also known that such features can be artifacts of the tomographic images. The possibility of the bright rim being solely an artifact caused by X-ray scattering at the solid–air interface was ruled out via additional analyses of the surface composition (see discussion in the SI). The presence of Cd in the outermost layer is interesting as this late order of precipitation does not follow the expected sequence of precipitation of the less-soluble endmember followed by the more-soluble endmember. Differences in the precipitation

kinetics of calcite and coprecipitated calcite may be playing a role in these observations, yet the ability to capture changes to physical features during nucleation and growth remains limited and further work remains to be done in this area of research.

For Zn at high concentration, the TXM image clearly reveals a high-density region in the particle center (Figure 4h), suggesting a high concentration of Zn as was evident in the μ XRF element maps (Figure 4f). This compositional gradient may be a result of early precipitation of the less-soluble Zn-rich calcium carbonate phase, leading to the later growth of a phase that is Ca-rich with preferential depletion of Zn from the solution. This drastic initial uptake of Zn in the calcite solid solution is expected based on the K_{sp} values of the endmembers (Table 1) and based on the phenomena of concentric zoning.⁶⁴ The TXM images of Zn–calcite particles

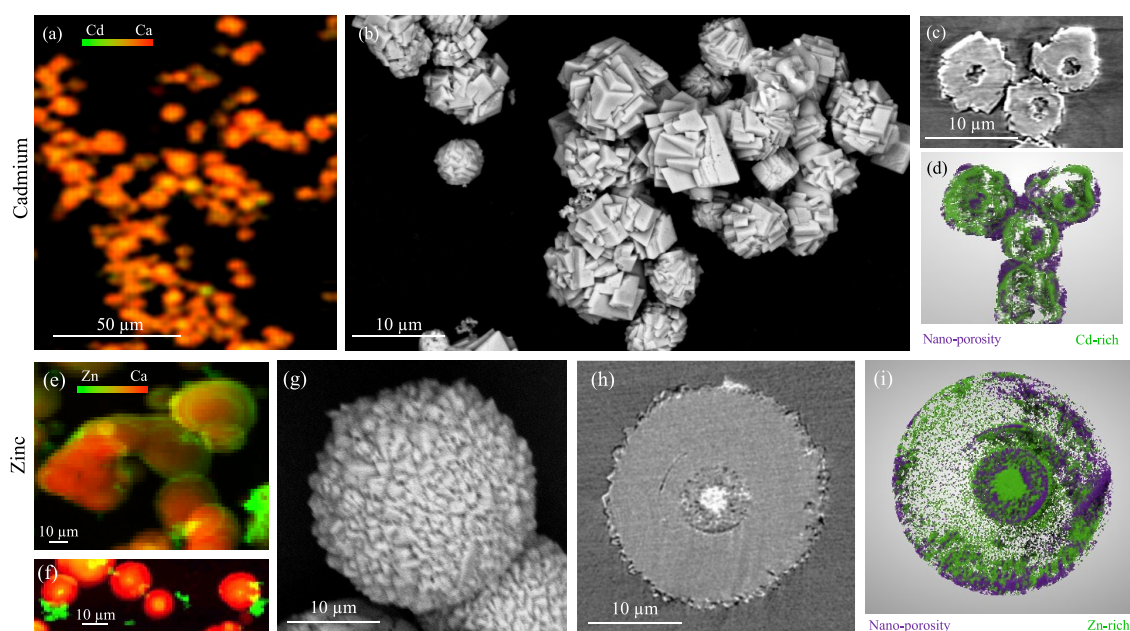


Figure 4. Imaging and analysis of carbonate precipitates after heavy metal uptake. μ XRF elemental mapping of Ca and heavy metals in precipitates from (a) $Cd_i = 0.02$ M and (f, g) $Zn_i = 0.02$ M experiments. Green represents Cd or Zn and red represents Ca. (b, g) SEM images of the Cd-calcite and Zn-calcite particles, respectively. (c, h) TXM images of internal structure where the bright spots indicate richness in Cd or Zn, relative to Ca. (d, i) 3D volume segmentation highlighting heavy metal-rich regions and nanoporosity within the particle.

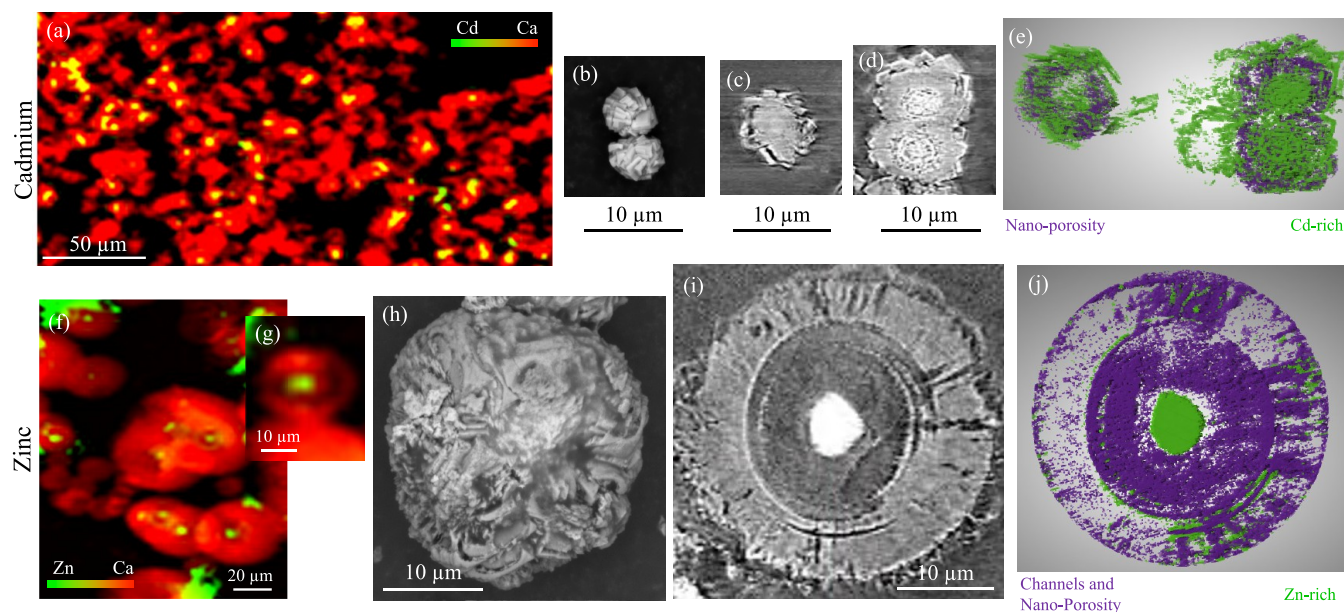


Figure 5. Imaging and analysis of carbonate precipitates after acid exposure. μ XRF elemental mapping of Ca and heavy metals in precipitates from (a) $Cd_i = 0.02$ M and (f, g) $Zn_i = 0.02$ M experiments. Green represents Cd or Zn and red represents Ca. (b, h) SEM images of the reacted Cd-calcite and Zn-calcite particles, respectively. (c, d, i) TXM images of internal structure where the bright spots indicate richness in Cd or Zn, relative to Ca. (e, j) 3D volume segmentation highlighting heavy metal-rich regions and nanoporosity within the particle. Note that these are not the same particles as the unreacted particles in Figure 4.

also show an intermediate layer that is more porous (Figure 4h). This layer is highlighted further in the volume segmentation image (Figure 4i). The presence of a slightly brighter outer rim is also captured in Figures 4h and S9b. Heterogeneity of incorporated trace elements within a single particle is presented at the μ m-scales with nm-resolutions, and segmentation based on the chemical gradients may be able to offer new explanations for the behavior of coprecipitated calcite in subsequent exposures to new solutions.

3.3. Concentrating of Heavy Metals in Calcite: Evaluation of Permanence under Acidic Conditions.

For all the experiments, ICP-MS measurements and mass balance calculations after acid exposure indicated minimal release of Cd and Zn back into solution. Mass retention was at least 95% of Cd and at least 88% of Zn for the highest concentration cases and 91% Cd and 84% Zn for the lowest concentration cases. The higher mass retention rates for Cd are expected based on relatively insoluble nature of otavite (Table

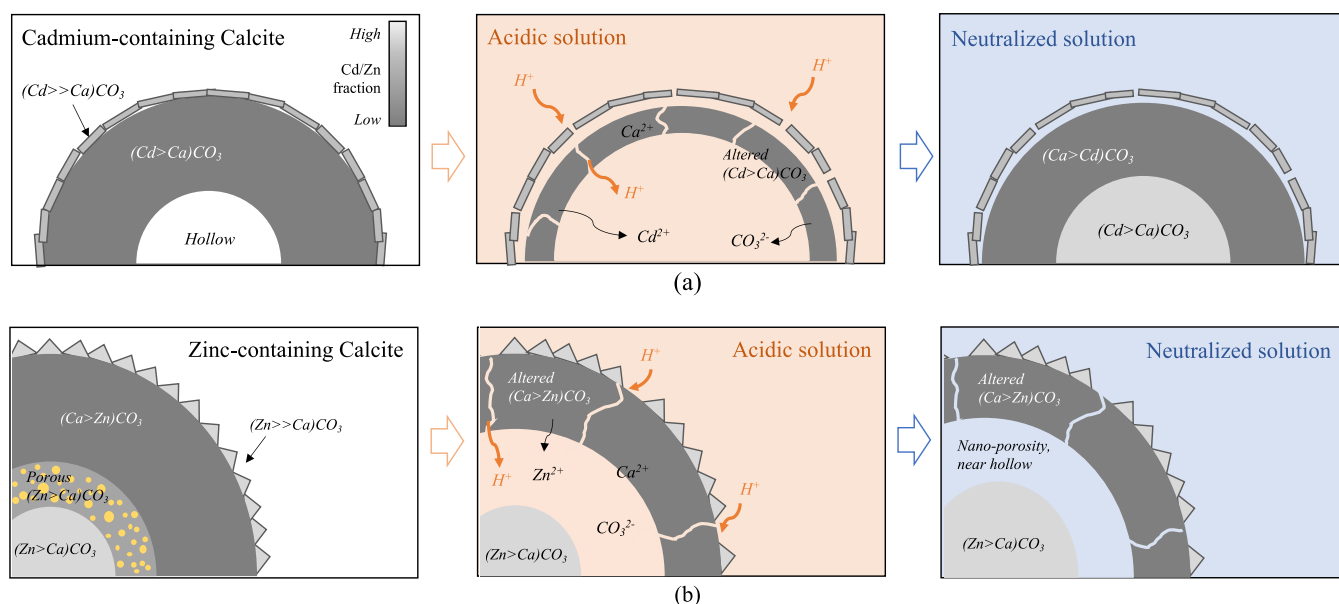


Figure 6. Conceptualization of the mechanisms of (a) Cd and (b) Zn reorganization during (orange background to indicate contact with acidic solution) and after acid exposure (blue background). In this figure, the lightest grayscale indicates the highest Cd or Zn concentration (as in the TXM images).

1). Heavy metal and Ca concentrations, along with the pH after 72 h, are presented in Table S1. The observed final pH at the end of 72 h was near neutral (Table S1), suggesting significant acid neutralization due to calcium leaching. In the long term, durable sequestration of heavy metals will depend on whether there is exposure to fresh acidic solutions. Nonetheless, these observations of selective calcium leaching suggest that the host carbonate can dissolve without jeopardizing the coprecipitated metals, at least initially.

The impacts of acid exposure on particle morphology, composition, and internal structure in highly Cd- and Zn-rich calcium carbonate precipitates are quite evident. Acid exposure did not lead to complete dissolution of the Cd- and Zn-calcites, and the same calcite peaks were consistently observed before and after the reaction in acid (Figure S11). Peaks belonging to hydrozincite were also consistently observed before and after acid exposure, indicating a minimal contribution of these phases to the total zinc release. For Cd-calcite particles, μ XRF maps show concentrating of Cd in the particle centers (Figure 5a), filling up what were initially hollow centers. Zinc also concentrated in the particle centers, more densely than in the unreacted particles, and μ XRF maps (Figure 5f,g) highlight the evident concentrating of heavy metals within the solid phase for several particles. Comparison of the μ XRF maps of high Zn-calcite batch before and after the reaction also shows a consistent presence of bright green areas, which are likely to be originating from unaltered hydrozincite phases present before acid exposure.

TXM imaging revealed significant alterations to the internal particle structure including etch pits deeply penetrating dissolution channels and internal hollow layers. The outer Cd-rich layer remained relatively intact upon acid exposure (Figure 5c,d). However, there is creation of a new porous layer underneath this outer layer (Figure 5c). We attribute this to the transport of acid through aggregated crystal boundaries,⁶⁵ which allowed for reaction within the particle interior. Figure 6 shows a conceptualization of the dissolution and reprecipitation processes during acid exposure. The reorganization of Cd

to the center likely occurred via dissolution of the internal calcite causing an increase in dissolved Ca and Cd concentration, which then led to Cd-enriched calcite precipitation until Cd depletion and ultimately precipitation of a Cd-poor calcite layer.

The Zn-calcite particles after acid exposure also exhibited many new features including channels connecting the bulk solution to the deep interior and significant nanoporosity generation in areas where there had been high Ca content and high porosity (Figure 5). Acid exposure yielded an increase in volume fraction of nanoporosity from approximately 3 to 26%, as estimated by quantification of the segmented volumes in the tomographic data. A mechanistic conceptualization of this process in comparison with that of Cd-calcite is shown in Figure 6. Transformation of Zn-rich calcites in acid is driven by creation of channels, which possibly served as conduits for water and ion transport, causing preferential dissolution of the more-soluble Ca-rich carbonate phases in the porous interior. This is likely to have increased the interior pH, which inhibited complete disintegration of the particle. Depletion of Ca in the interior allowed for enlargement of the already-existing Zn-rich carbonate core.

Our inference suggests that dissolution mechanism and heavy metal retention processes are controlled by the substructure and compositional gradient within particles. The presence of multiple layers of variable chemical compositions allowed for concentrating or reprecipitation within a single particle rather than dissolution as predicted by SS-AS theory. While the single particle imaging technique limits our ability to generalize far beyond the samples imaged and the two cases analyzed, it stands to reason that for other cations belonging to the rhombohedral carbonates and those that are less soluble than calcite (i.e., rhodochrosite or siderite), selective release of calcium may drive the process of metal retention.

These findings also imply that the dissolution rate of coprecipitated calcite can vary spatially as the reaction front interacts with different layers of the precipitate (Figure 6). For example, there may be inhibiting effects on dissolution with an

increasing fraction of the heavy metal or the opposite effects with an increasing degree of nanoporosity. Overall, the spatial distribution of the heavy metals and porosity within particles will impact the congruency of coprecipitated element release and the overall reactivity of the mineral phases. Further work remains to be done to separate out the rates of calcite dissolution within nonhomogeneous, coprecipitated calcium carbonate phases.

4. ENVIRONMENTAL SIGNIFICANCE

The results of this work serve to inspire innovation in engineered strategies for removing heavy metals from water, considering co-benefits for CO₂ sequestration in highly contaminated waste sites and waste materials such as combustion ash. Cd and Zn concentrations in synthetic waste leachates were reduced by more than two orders of magnitude after one cycle of induced calcium carbonate precipitation, highlighting the effectiveness of carbonate precipitation for treatment of highly contaminated solutions. Multiple cycles of carbonate precipitation are likely to lead to solutions that meet the MCL set by the U.S. EPA, and our results show that the fractional removal of metals is largely independent of the initial heavy metal concentration (Figure 2).

Initial coprecipitation of Cd and Zn exhibited different behaviors from each other, and our nanometer-scale characterizations revealed previously unseen internal features (i.e., porosity and chemical gradient) of coprecipitated calcites. These novel findings provide a context through which we can understand the retention of coprecipitated heavy metals upon acid exposure, with nearly 95% Zn mass retention and 88% Cd mass retention. Specifically, the TXM imaging show that coprecipitated heavy metals were found to be concentrated deep inside the precipitates after acid exposure rather than be released, which we infer was enabled by the internal structure of the coprecipitates. These results further motivate applications of engineered carbonate precipitation in not only alkaline waste sites but also acidic waste sites. Still, the longevity of the mineralized metals with ongoing exposure to fresh acidic solutions remains to be studied. With careful engineered controls of pH and with the presence of other dissolved species, it can be speculated that subsequent mineral replacement reactions involving precipitation of less-reactive phases on the surface of coprecipitated calcium carbonates^{65,66} may lead to further stabilization of calcium carbonate from continued and complete dissolution.

The experiments reported here are the first attempts to gain foundational knowledge for scaling up to coprecipitation in more complex, polyionic solutions, as previous research revealed complexities in simultaneous cation and anion uptake in calcium carbonate systems.²⁰ If the observations of uptake and stabilization of coprecipitated elements can be extended to other calcium carbonate polymorphs (i.e., aragonite or vaterite), this process can be used to target the treatment of other divalent cations that belong to aragonite or vaterite crystal groups (i.e., Pb, Ba, or Sr). Findings here may be further applicable to the recovery of critical elements such as Co, Mg, Ni, and Li, which are known to coprecipitate with calcium carbonate,^{10,67–69} if coupled with a two-step process of carbon mineralization followed by engineered acid exposure for in-situ, long-term passive treatment for stabilization and subsequent recovery.

■ ASSOCIATED CONTENT

Supporting Information

The Supporting Information is available free of charge at <https://pubs.acs.org/doi/10.1021/acs.est.2c07678>.

Heavy metal uptake % with calcium concentration (Figure S1); Lippmann diagrams for the Cd and Zn experiments (Figure S2); XRD patterns of low Cd and low Zn carbonates (Figure S3); plots of FWHM vs momentum transfer (Figure S4); SEM image of the calcite control sample (Figure S5); TXM/XRF data from control and low Cd- and Zn- calcites (Figure S6); intensity plots over a single particle for unreacted and reacted Cd- and Zn-carbonates (Figures S7 and S9); energy-dispersive X-ray spectroscopy spectrum and quantification for Cd- and Zn- carbonates (Figures S8 and S10); XRD patterns comparing reacted and unreacted Cd- and Zn-calcites; XRD patterns of reacted calcites (Figure S11); 3D animations and fly-through scans of unreacted and reacted Cd- and Zn-carbonates (Movies S1–S8 and Figures S12 and S13 (snapshots)) (PDF)

■ AUTHOR INFORMATION

Corresponding Author

Catherine A. Peters – Department of Civil and Environmental Engineering, Princeton University, Princeton, New Jersey 08544, United States; orcid.org/0000-0003-2418-795X; Email: cap@princeton.edu

Authors

Julie J. Kim – Department of Civil and Environmental Engineering, Princeton University, Princeton, New Jersey 08544, United States; orcid.org/0000-0002-9854-5898
Sang Soo Lee – Chemical Sciences and Engineering Division, Argonne National Laboratory, Lemont, Illinois 60439, United States; orcid.org/0000-0001-8585-474X
Paul Fenter – Chemical Sciences and Engineering Division, Argonne National Laboratory, Lemont, Illinois 60439, United States; orcid.org/0000-0002-6672-9748
Satish C. B. Myneni – Department of Geosciences, Princeton University, Princeton, New Jersey 08544, United States
Viktor Nikitin – Advanced Photon Source, Argonne National Laboratory, Lemont, Illinois 60439, United States

Complete contact information is available at:

<https://pubs.acs.org/10.1021/acs.est.2c07678>

Author Contributions

The manuscript was written through contributions of all authors. All authors have given approval to the final version of the manuscript.

Notes

The authors declare no competing financial interest.

■ ACKNOWLEDGMENTS

This material is based upon work supported by the U.S. Department of Energy, Office of Science, Office of Workforce Development for Teachers and Scientists, Office of Science Graduate Student Research (SCGSR) program. The SCGSR program is administered by the Oak Ridge Institute for Science and Education (ORISE) for the DOE. ORISE is managed by ORAU under contract number DE-SC0014664. All opinions expressed in this paper are the author's and do not necessarily

reflect the policies and views of DOE, ORAU, or ORISE. Support also came from Princeton University through the High Meadows Environmental Institute as part of the Water Grand Challenges initiative, and through a SEAS Innovation Grant from the Moore Charitable Foundation. PF and SSL were supported by U.S. Department of Energy, Office of Science, Office of Basic Energy Sciences, Chemical Sciences, Geosciences, and Biosciences Division (Geosciences subprogram) at Argonne National Laboratory. This research used beamlines 32-ID, 13-ID-E, and 11-BM of the Advanced Photon Source, a U.S. Department of Energy (DOE) Office of Science user facility at Argonne National Laboratory and is based on research supported by the U.S. DOE Office of Science-Basic Energy Sciences, under Contract No. DE-AC02-06CH11357. The portions of this work that were performed at GeoSoilEnviroCARS (The University of Chicago, Sector 13), Advanced Photon Source (APS), Argonne National Laboratory were supported by the National Science Foundation – Earth Sciences (EAR – 1634415) and Department of Energy-GeoSciences (DE-FG02-94ER14466). The authors acknowledge Antonio Lanzirrotti and Matt Newville for their assistance in collecting the μ XRF- μ XRD data, as well as Stefania Gili and Yifen Tsai for collecting the ICP-MS data.

■ ABBREVIATIONS

TXM	transmission X-ray microscopy
XRD	X-ray diffraction
XRF	X-ray fluorescence
ICP-MS	inductively coupled plasma mass spectrometry
SEM	scanning electron microscopy

■ REFERENCES

- (1) Schwartz, G. E.; Hower, J. C.; Phillips, A. L.; Rivera, N.; Vengosh, A.; Hsu-Kim, H. Ranking Coal Ash Materials for Their Potential to Leach Arsenic and Selenium: Relative Importance of Ash Chemistry and Site Biogeochemistry. *Environ. Eng. Sci.* **2018**, *35*, 728–738.
- (2) Izquierdo, M.; Querol, X. Leaching Behaviour of Elements from Coal Combustion Fly Ash: An Overview. *Int. J. Coal Geol.* **2012**, *94*, 54–66.
- (3) Blowes, D. W.; Ptacek, C. J.; Jambor, J. L.; Weisener, C. G.; Paktunc, D.; Gould, W. D.; Johnson, D. B. The Geochemistry of Acid Mine Drainage. In *Treatise on Geochemistry*, 11th ed.; Elsevier Ltd, 2003; Vol. 11, pp 131–190.
- (4) Naicker, K.; Cukrowska, E.; McCarthy, T. S. Acid Mine Drainage Arising from Gold Mining Activity in Johannesburg, South Africa and Environs. *Environ. Pollut.* **2003**, *122*, 29–40.
- (5) Nordstrom, D. K. Mine Waters: Acidic to Circumneutral. *Elements* **2011**, *7*, 393–398.
- (6) Nyquist, J.; Greger, M. A Field Study of Constructed Wetlands for Preventing and Treating Acid Mine Drainage. *Ecol. Eng.* **2009**, *35*, 630–642.
- (7) RoyChowdhury, A.; Sarkar, D.; Datta, R. Remediation of Acid Mine Drainage-Impacted Water. *Curr. Pollut. Rep.* **2015**, *1*, 131–141.
- (8) Skousen, J. G.; Ziemkiewicz, P. F.; McDonald, L. M. Acid Mine Drainage Formation, Control and Treatment: Approaches and Strategies. *Extr. Ind. Soc.* **2019**, *6*, 241–249.
- (9) Middleton, A.; Park, D. M.; Jiao, Y.; Hsu-Kim, H. Major Element Composition Controls Rare Earth Element Solubility during Leaching of Coal Fly Ash and Coal By-Products. *Int. J. Coal Geol.* **2020**, *227*, No. 103532.
- (10) Hassas, B. V.; Rezaee, M.; Pisupati, S. V. Precipitation of Rare Earth Elements from Acid Mine Drainage by CO₂ Mineralization Process. *Chem. Eng. J.* **2020**, *399*, No. 125716.
- (11) McCutcheon, J.; Dipple, G. M.; Wilson, S. A.; Southam, G. Production of Magnesium-Rich Solutions by Acid Leaching of Chrysotile: A Precursor to Field-Scale Deployment of Microbially Enabled Carbonate Mineral Precipitation. *Chem. Geol.* **2015**, *413*, 119–131.
- (12) Bullock, L. A.; James, R. H.; Matter, J.; Renforth, P.; Teagle, D. A. H. Global Carbon Dioxide Removal Potential of Waste Materials From Metal and Diamond Mining. *Front. Clim.* **2021**, *3*, No. 77.
- (13) Renforth, P. The Negative Emission Potential of Alkaline Materials. *Nat. Commun.* **2019**, *10*, No. 1401.
- (14) Kirchofer, A.; Becker, A.; Brandt, A.; Wilcox, J. CO₂ Mitigation Potential of Mineral Carbonation with Industrial Alkalinity Sources in the United States. *Environ. Sci. Technol.* **2013**, *47*, 7548–7554.
- (15) Li, J.; Hitch, M.; Power, I.; Pan, Y. Integrated Mineral Carbonation of Ultramafic Mine Deposits-A Review. *Minerals* **2018**, *8*, No. 147.
- (16) Bullock, L. A.; Yang, A.; Darton, R. C. Kinetics-Informed Global Assessment of Mine Tailings for CO₂ Removal. *Sci. Total Environ.* **2022**, *808*, No. 152111.
- (17) Narode, A.; Pour-Ghaz, M.; Ducoste, J. J.; Barlaz, M. A. Measurement of Heat Release during Hydration and Carbonation of Ash Disposed in Landfills Using an Isothermal Calorimeter. *Waste Manage.* **2021**, *124*, 348–355.
- (18) Hitch, M.; Dipple, G. M. Economic Feasibility and Sensitivity Analysis of Integrating Industrial-Scale Mineral Carbonation into Mining Operations. *Miner. Eng.* **2012**, *39*, 268–275.
- (19) Hamilton, J. L.; Wilson, S. A.; Morgan, B.; Turvey, C. C.; Paterson, D. J.; MacRae, C.; McCutcheon, J.; Southam, G. Nesquehonite Sequesters Transition Metals and CO₂ during Accelerated Carbon Mineralisation. *Int. J. Greenhouse Gas Control* **2016**, *55*, 73–81.
- (20) Hunter, H. A.; Ling, F. T.; Peters, C. A. Coprecipitation of Heavy Metals in Calcium Carbonate from Coal Fly Ash Leachate. *ACS ES&T Water* **2021**, *1*, 339–345.
- (21) Prieto, M.; Heberling, F.; Rodríguez-Galán, R. M.; Brandt, F. Crystallization Behavior of Solid Solutions from Aqueous Solutions: An Environmental Perspective. *Prog. Cryst. Growth Charact. Mater.* **2016**, *62*, 29–68.
- (22) Drake, H.; Mathurin, F. A.; Zack, T.; Schäfer, T.; Roberts, N. M. W.; Whitehouse, M.; Karlsson, A.; Broman, C.; Åström, M. E. Incorporation of Metals into Calcite in a Deep Anoxic Granite Aquifer. *Environ. Sci. Technol.* **2018**, *52*, 493–502.
- (23) Tobin, K. J.; Colwell, F. S.; Onstott, T. C.; Smith, R. Recent Calcite Spar in an Aquifer Waste Plume: A Possible Example of Contamination Driven Calcite Precipitation. *Chem. Geol.* **2000**, *169*, 449–460.
- (24) Balboni, E.; Smith, K. F.; Moreau, L. M.; Wimpenny, J.; Booth, C. H.; Kersting, A. B.; Zavarin, M. Plutonium Co-Precipitation with Calcite. *ACS Earth Space Chem.* **2021**, *5*, 3362–3374.
- (25) Prieto, M. Thermodynamics of Solid Solution Aqueous Solution Systems. *Rev. Mineral. Geochem.* **2009**, *70*, 47–85.
- (26) Crocket, J. H.; Winchester, J. W. Coprecipitation of Zinc with Calcium Carbonate. *Geochim. Cosmochim. Acta* **1966**, *30*, 1093–1109.
- (27) Lorens, R. B. Sr, Cd, Mn and Co Distribution Coefficients in Calcite as a Function of Calcite Precipitation Rate. *Geochim. Cosmochim. Acta* **1981**, *45*, 553–561.
- (28) Davis, J. A.; Fuller, C. C.; Cook, A. D. A Model for Trace Metal Sorption Processes at the Calcite Surface: Adsorption of Cd²⁺ and Subsequent Solid Solution Formation. *Geochim. Cosmochim. Acta* **1987**, *51*, 1477–1490.
- (29) Tesoriero, A. J.; Pankow, J. F. Solid Solution Partitioning of Sr²⁺, Ba²⁺, and Cd²⁺ to Calcite. *Geochim. Cosmochim. Acta* **1996**, *60*, 1053–1063.
- (30) Temmam, M.; Paquette, J.; Vali, H. Mn and Zn Incorporation into Calcite as a Function of Chloride Aqueous Concentration. *Geochim. Cosmochim. Acta* **2000**, *64*, 2417–2430.
- (31) Katsikopoulos, D.; Fernandez-Gonzalez, Á.; Prieto, M. Crystallization of the (Cd,Ca)CO₃ Solid Solution in Double Diffusion Systems: The Partitioning Behaviour of Cd²⁺ in Calcite at Different Supersaturation Rates. *Mineral. Mag.* **2008**, *72*, 433–436.

- (32) Li, X.; Zhang, Q.; Yang, B. Co-Precipitation with CaCO₃ to Remove Heavy Metals and Significantly Reduce the Moisture Content of Filter Residue. *Chemosphere* **2020**, *239*, No. 124660.
- (33) Prieto, M.; Fernández-González, A.; Putnis, A.; Fernández-Díaz, L. Nucleation, Growth, and Zoning Phenomena in Crystallizing (Ba,Sr)CO₃, Ba (SO₄,CrO₄), (Ba,Sr)SO₄, and (Cd,Ca)CO₃ Solid Solutions from Aqueous Solutions. *Geochim. Cosmochim. Acta* **1997**, *61*, 3383–3397.
- (34) Ma, C.; Xu, F.; Zhu, Z.; Yang, H.; Nong, P.; Kang, Z.; Tang, S.; Zhang, L.; Zhu, Y. Dissolution and Solubility of the Calcite–Otavite Solid Solutions [(Ca_{1-x}Cd_x)CO₃] at 25 °C. *Minerals* **2022**, *12*, No. 756.
- (35) Glynn, P. D.; Reardon, E. J.; Plummer, L. N.; Busenberg, E. Reaction Paths and Equilibrium End-Points in Solid-Solution Aqueous-Solution Systems. *Geochim. Cosmochim. Acta* **1990**, *54*, 267–282.
- (36) Godelitsas, A.; Astilleros, J. M. Dissolution, Sorption/(Re)Precipitation, Formation of Solid Solutions and Crystal Growth Phenomena on Mineral Surfaces: Implications for the Removal of Toxic Metals from the Environment. In *Ion Partitioning in Ambient-Temperature Aqueous Systems* 2010; Vol. 10, pp 289–324.
- (37) Prieto, M.; Astilleros, J. M.; Fernández-Díaz, L. Environmental Remediation by Crystallization of Solid Solutions. *Elements* **2013**, *9*, 195–201.
- (38) Ling, F. T.; Hunter, H. A.; Fitts, J. P.; Peters, C. A.; Acerbo, A. S.; Huang, X.; Yan, H.; Nazaretski, E.; Chu, Y. S. Nanospectroscopy Captures Nanoscale Compositional Zonation in Barite Solid Solutions. *Sci. Rep.* **2018**, *8*, No. 13041.
- (39) Hunter, H. A.; Ling, F. T.; Peters, C. A. Metals Coprecipitation with Barite: Nano-XRF Observation of Enhanced Strontium Incorporation. *Environ. Eng. Sci.* **2020**, *37*, 235–245.
- (40) Ghizellaoui, S.; Euvrard, M. Assessing the Effect of Zinc on the Crystallization of Calcium Carbonate. *Desalination* **2008**, *220*, 394–402.
- (41) Gonçalves, M. A.; Prieto, M. Development of Compositional Patterns during the Growth of Solid Solutions from Aqueous Solutions: A Cellular Automaton Simulation. *Cryst. Growth Des.* **2014**, *14*, 2782–2793.
- (42) Mergelsberg, S. T.; Riechers, S. L.; Graham, T. R.; Prange, M. P.; Kerisit, S. N. Effect of Cd on the Nucleation and Transformation of Amorphous Calcium Carbonate. *Cryst. Growth Des.* **2021**, *21*, 3384–3393.
- (43) Deonaraine, A.; Kolker, A.; Foster, A. L.; Doughten, M. W.; Holland, J. T.; Bailoo, J. D. Arsenic Speciation in Bituminous Coal Fly Ash and Transformations in Response to Redox Conditions. *Environ. Sci. Technol.* **2016**, *50*, 6099–6106.
- (44) Fashola, M. O.; Ngole-Jeme, V. M.; Babalola, O. O. Heavy Metal Pollution from Gold Mines: Environmental Effects and Bacterial Strategies for Resistance. *Int. J. Environ. Res. Public Health* **2016**, *13*, No. 1047.
- (45) Ko, I.; Ahn, J. S.; Park, Y. S.; Kim, K. W. Arsenic Contamination of Soils and Sediments from Tailings in the Vicinity of Myungbong Au Mine, Korea. *Chem. Speciation Bioavailability* **2003**, *15*, 67–74.
- (46) Lange, C. N.; Flues, M.; Hiromoto, G.; Boscov, M. E. G.; Camargo, I. M. C. Long-Term Leaching of As, Cd, Mo, Pb, and Zn from Coal Fly Ash in Column Test. *Environ. Monit. Assess.* **2019**, *191*, No. 602.
- (47) Lee, G.; Bigham, J. M.; Faure, G. Removal of Trace Metals by Coprecipitation with Fe, Al and Mn from Natural Waters Contaminated with Acid Mine Drainage in the Ducktown Mining District, Tennessee. *Appl. Geochem.* **2002**, *17*, 569–581.
- (48) Sun, C.; Chen, J.; Tian, K.; Peng, D.; Liao, X.; Wu, X. Geochemical Characteristics and Toxic Elements in Alumina Refining Wastes and Leachates from Management Facilities. *Int. J. Environ. Res. Public Health* **2019**, *16*, No. 1297.
- (49) Ball, J. W.; Nordstrom, D. K. *User's Manual for WATEQ. 4F*, Database - US Geological Survey Open-File Report, 1991; pp 91–183.
- (50) Catalano, J. G.; Huhmann, B. L.; Luo, Y.; Mitnick, E. H.; Slavney, A.; Giammar, D. E. Metal Release and Speciation Changes during Wet Aging of Coal Fly Ashes. *Environ. Sci. Technol.* **2012**, *46*, 11804–11812.
- (51) De Andrade, V.; Nikitin, V.; Wojcik, M.; Deriy, A.; Bean, S.; Shu, D.; Mooney, T.; Peterson, K.; Kc, P.; Li, K.; Ali, S.; Fezzaa, K.; Gürsoy, D.; Arico, C.; Ouendi, S.; Troadec, D.; Simon, P.; De Carlo, F.; Lethien, C. Fast X-Ray Nanotomography with Sub-10 Nm Resolution as a Powerful Imaging Tool for Nanotechnology and Energy Storage Applications. *Adv. Mater.* **2021**, *33*, No. 2008653.
- (52) Gürsoy, D.; De Carlo, F.; Xiao, X.; Jacobsen, C. TomoPy: A Framework for the Analysis of Synchrotron Tomographic Data. *J. Synchrotron Radiat.* **2014**, *21*, 1188–1193.
- (53) Nikitin, V. TomocuPy – Efficient GPU-Based Tomographic Reconstruction with Asynchronous Data Processing. *J. Synchrotron Radiat.* **2023**, *30*, 179–191.
- (54) Newville, M. Larch: An Analysis Package for XAFS and Related Spectroscopies. *J. Phys.: Conf. Ser.* **2013**, *430*, No. 012007.
- (55) Nehrke, G.; Reichart, G. J.; Van Cappellen, P.; Meile, C.; Bijma, J. Dependence of Calcite Growth Rate and Sr Partitioning on Solution Stoichiometry: Non-Kossel Crystal Growth. *Geochim. Cosmochim. Acta* **2007**, *71*, 2240–2249.
- (56) Astilleros, J. M.; Fernández-Díaz, L.; Putnis, A. The Role of Magnesium in the Growth of Calcite: An AFM Study. *Chem. Geol.* **2010**, *271*, 52–58.
- (57) Davis, K. J.; Dove, P. M.; De Yoreo, J. J. The Role of Mg²⁺ as an Impurity in Calcite Growth. *Science* **2000**, *290*, 1134–1137.
- (58) Zhang, X.; Guo, J.; Wu, S.; Chen, F.; Yang, Y. Divalent Heavy Metals and Uranyl Cations Incorporated in Calcite Change Its Dissolution Process. *Sci. Rep.* **2020**, *10*, No. 16864.
- (59) Alwan, A. K.; Williams, P. A. Mineral Formation from Aqueous Solution. Part I. The Deposition of Hydrozincite, Zn₅(OH)₆(CO₃)₂, from Natural Waters. *Transition Met. Chem.* **1979**, *4*, 128–132.
- (60) Sibrell, P. L.; Chambers, M. A.; Deaguero, A. L.; Wildeman, T. R.; Reisman, D. J. An Innovative Carbonate Coprecipitation Process for the Removal of Zinc and Manganese from Mining Impacted Waters. *Environ. Eng. Sci.* **2007**, *24*, 881–895.
- (61) Köhler, S. J.; Cubillas, P.; Rodríguez-Blanco, J. D.; Bauer, C.; Prieto, M. Removal of Cadmium from Wastewaters by Aragonite Shells and the Influence of Other Divalent Cations. *Environ. Sci. Technol.* **2007**, *41*, 112–118.
- (62) Tomioka, T.; Fuji, M.; Takahashi, M.; Takai, C.; Utsuno, M. Hollow Structure Formation Mechanism of Calcium Carbonate Particles Synthesized by the CO₂ Bubbling Method. *Cryst. Growth Des.* **2012**, *12*, 771–776.
- (63) Hadiko, G.; Han, Y. S.; Fuji, M.; Takahashi, M. Synthesis of Hollow Calcium Carbonate Particles by the Bubble Templating Method. *Mater. Lett.* **2005**, *59*, 2519–2522.
- (64) Fernández-González, A.; Prieto, M.; Putnis, A.; López-Andrés, S. Concentric Zoning Patterns in Crystallizing (Cd,Ca)CO₃ Solid Solutions from Aqueous Solutions. *Mineral. Mag.* **1999**, *63*, 331–343.
- (65) Kim, Y.; Abdilla, B.; Yuan, K.; De Andrade, V.; Sturchio, N. C.; Lee, S. S.; Fenter, P. Replacement of Calcium Carbonate Polymorphs by Cerussite. *ACS Earth Space Chem.* **2021**, *5*, 2433–2441.
- (66) Kim, Y. J.; Tekawade, A.; Lee, S. S.; Fenter, P. Morphological and Crystallographic Controls in the Replacement of Calcite and Aragonite by Cerussite and Otavite. *Geochim. Cosmochim. Acta* **2023**, *341*, 16–27.
- (67) Füger, A.; Konrad, F.; Leis, A.; Dietzel, M.; Mavromatis, V. Effect of Growth Rate and PH on Lithium Incorporation in Calcite. *Geochim. Cosmochim. Acta* **2019**, *248*, 14–24.
- (68) Terakado, Y.; Masuda, A. The Coprecipitation of Rare-Earth Elements with Calcite and Aragonite. *Chem. Geol.* **1988**, *69*, 103–110.
- (69) Miranda, M. M.; Bielicki, J. M.; Chun, S.; Cheng, C.-M. Recovering Rare Earth Elements from Coal Mine Drainage Using Industrial Byproducts: Environmental and Economic Consequences. *Environ. Eng. Sci.* **2022**, *39*, 770–783.